

 Open access • Journal Article • DOI:10.1021/ACSNANO.6B01944

Graphene as a Tunable Anisotropic or Isotropic Plasmonic Metasurface.

— [Source link](#) 

Paloma A. Huidobro, Matthias Kraft, Stefan A. Maier, John B. Pendry





Institutions: Imperial College London

Published on: 25 Apr 2016 - ACS Nano (American Chemical Society)

Topics: Metamaterial, Graphene and Plasmon

Related papers:

- [Graphene plasmonics for tunable terahertz metamaterials](#)
- [Graphene Plasmonics: A Platform for Strong Light-Matter Interactions](#)
- [Graphene plasmonics: A platform for strong light-matter interaction](#)
- [Transformation Optics Using Graphene](#)
- [Gate-tuning of graphene plasmons revealed by infrared nano-imaging](#)

Share this paper:    

View more about this paper here: <https://typeset.io/papers/graphene-as-a-tunable-anisotropic-or-isotropic-plasmonic-xdnhluzyau>

Graphene as a Tunable Anisotropic or Isotropic Plasmonic Metasurface

Paloma A. Huidobro,* Matthias Kraft, Stefan A. Maier, and John B. Pendry

*Imperial College London, Department of Physics, The Blackett Laboratory, London SW7
2AZ, UK*

E-mail: p.arroyo-huidobro@imperial.ac.uk

Abstract

We demonstrate a tunable plasmonic metasurface by considering a graphene sheet subject to a periodically patterned doping level. The unique optical properties of graphene result in electrically tunable plasmons that allow for extreme confinement of electromagnetic energy in the technologically significant regime of THz frequencies. Here we add an extra degree of freedom by using graphene as a metasurface, proposing to dope it with an electrical gate patterned in the micron or sub-micron scale. By extracting the effective conductivity of the sheet we characterize metasurfaces periodically modulated along one or two directions. In the first case, and making use of the analytical insight provided by transformation optics, we show an efficient control of THz radiation for one polarization. In the second case, we demonstrate a metasurface with an isotropic response that is independent of wave polarization and orientation.

Graphene, an atomically-thin layer of carbon atoms arranged in a honeycomb lattice, features outstanding mechanical, thermal and electrical properties.¹ Its characteristic linear

*To whom correspondence should be addressed

dispersion for electrons close to the Dirac point results in the possibility of tuning the carrier concentration by external means.² In particular, graphene can be biased by electrical gating or surface doping, which modifies its Fermi level and permits the existence of surface plasmons propagating along graphene. Because of the two-dimensional (2D) nature of this material, the surface plasmons it supports have very short wavelengths and exhibit extreme out-of-plane confinement to the sheet, as has already been demonstrated in a number of experiments.³⁻¹¹

Compared to the noble metals commonly employed for plasmonics,¹² graphene has a low carrier concentration, and, for this reason, plasmons in graphene are relatively long-lived and appear at lower frequencies. While the plasmonic response of metals is weak at the infrared or lower frequencies, graphene plasmons exist in the THz regime with relatively low losses.¹³⁻¹⁵ These facts, added to the important ingredient of tunability, make graphene a very suitable platform for the design of plasmonic metasurfaces in the THz regime.^{16,17} Metasurfaces, the 2D counterpart of metamaterials,^{18,19} consist of a planar arrangement of resonant subwavelength-sized building blocks.²⁰ By appropriately designing the blocks and their arrangement, metasurfaces provide an ultra-thin platform for manipulating electromagnetic (EM) waves. Novel phenomena and applications based on metasurfaces range from broadband light bending and anomalous reflection and refraction²¹⁻²³ to strong spin-orbit interactions of light.²⁴

In this work, we study graphene as a plasmonic metasurface that offers the potential to control radiation in the THz regime. Different from previous studies,^{16,17} which focused on patterning the graphene, here we consider a continuous graphene sheet with periodically modulated doping. This gives rise to the possibility of an electrically tunable metasurface that can be used to dynamically control radiation in the THz regime. First, we consider a graphene sheet with doping modulation in one direction. We choose very general sinusoidal doping patterns, and we focus on the electric dipole mode that is visible even for highly lossy graphene samples. We show that the coupling to surface plasmons greatly enhances

the interaction of graphene with radiation and we characterize the system as a metasurface with an effective surface conductivity. With the help of transformation optics, we give an analytical expression for the effective conductivity at normal incidence. Next, we consider a graphene monolayer with doping modulated along two directions, and discuss how, thanks to plasmons, transmission of EM waves can be greatly suppressed independently of wave polarization and angle of incidence.

In our calculations, we model the graphene as a 2D sheet characterised by an electrical conductivity $\sigma_g(\omega)$. Since we focus at THz frequencies, we use the Drude model for the conductivity

$$\sigma_g(\omega) = \frac{\alpha}{\gamma_g - i\omega}, \quad (1)$$

where $\alpha = e^2\mu/\pi\hbar^2$ is the Drude weight and $\gamma_g = 1/\tau$ is the collision frequency. Here, μ and τ are the chemical potential and the scattering time for electrons, respectively, with $\tau = m\mu/ev_F^2$ (m is the mobility and $v_F \approx 10^6$ m/s the Fermi velocity). This formula, which neglects interband contributions to the conductivity, is a very good approximation to the full conductivity obtained from the RPA at sufficiently low frequencies and high dopings (see SM for a detailed comparison). In this work, we use the parameters $\alpha = 76$ GHz/ Ω and $\gamma = 1.5$ THz, which correspond to the generally used values $\mu = 0.65$ eV and $m = 10^4$ cm²/V s, see *e.g.* Ref. 25. In addition, and in order to show that our results are general and our fundamental conclusions do not depend on the particular choice of parameters for graphene, we present results for graphene with $\alpha = 76$ GHz/ Ω and $\gamma = 9.8$ THz ($\mu = 0.65$ eV, $m = 1.6 \times 10^3$ cm²/V s and $\tau = 0.1$ ps) in the SM, taken from experimental data²⁶ and used in Ref. 16.

Graphene with 1D conductivity modulation

The configuration we first consider is sketched in Fig. 1(a). A graphene monolayer is placed between two dielectrics, ϵ_1 and ϵ_2 , and biased in a way that results in a periodic modulation

of the conductivity of the sheet along one direction (the x -axis). This can be done by, for instance, biasing the graphene with a periodic electrostatic field. The most general class of conductivity modulation achieved with a periodic bias can be described by a sinusoidal as,

$$\sigma(x) = \sigma_g \left(a_0 + a_1 \sin \frac{x}{2\pi\gamma} \right), \quad (2)$$

where σ_g is the conductivity of the homogeneously biased graphene (Eq. 1), $2\pi\gamma$ is the periodicity and $\{a_0, a_1\}$ are two parameters related to the strength of the modulation. This periodic modulation of the conductivity acts as a grating that supplies the momentum mismatch for free space radiation to couple into the surface plasmons sustained by the graphene layer, which have much shorter wavelength. In fact, since the momentum of the graphene plasmons is much larger than that of the radiation, the modulation period needs to be much smaller than the incident wavelength ($\lambda \gg 2\pi\gamma$). Such coupling of radiation into graphene plasmons has already been shown both theoretically^{27,28} and experimentally.²⁹ Alternatively, other works have shown coupling through relief corrugations or subwavelength gratings on which graphene is placed,³⁰⁻³⁴ as well as patterned graphene structures including 1D arrays of micro-ribbons^{13,35} and 2D arrangements of islands.^{25,36-38} In order to achieve a periodic doping in the graphene, the sheet can be biased with the spatially periodic electrostatic field generated by a periodically corrugated plane, either metallic or dielectric (see Fig. S2 in the SM). The doping can then be dynamically tuned by adjusting the gate potential. Compared to directly patterning graphene, this approach takes advantage of state-of-the-art fabrication techniques to pattern metal and dielectric films in the sub-micron scale. Note that we do not include the patterned film in our calculations as it has no effect on the near field of the graphene, see for instance Ref. 39

In the subwavelength regime, the modulated graphene sheet appears as a homogeneous 1D layer for the incident radiation, that is, a metasurface characterised by an effective electrical conductivity σ_{eff} , see the right-hand side panel in Fig. 1(a). The effective response

of this graphene metasurface under the incidence of a p-polarised EM wave ($\mathbf{H} = H\mathbf{u}_z$) can be derived analytically with the help of transformation optics. A graphene sheet with the conductivity profile $\sigma(x)$ can be mapped to a simpler system by means of the following conformal transformation,^{28,40}

$$z = \gamma \log \left(\frac{1}{e^w - iw_0} + iy_0 \right), \quad (3)$$

which maps a Cartesian space ($w = u + iv$) to a wavy mesh ($z = x + iy$) that is periodic along x . Hence, it relates a simple flat and homogeneously biased graphene sheet in z -space to a periodically biased graphene monolayer in w -space.²⁸ In the above equation, γ is a scaling factor that yields the periodicity in z -space, w_0 represents the modulation strength and $y_0 = \frac{w_0}{e^{2b} - w_0^2}$, where b is a parameter that represents the position of the graphene layer in the w -space. Figure 1(b) shows the conductivity modulation profile derived from the conformal transformation for different modulation strengths (plotted with solid lines). In addition, the dots represent the conductivity modulation, but for the simple sinusoidal expression in Eq. 2, with $\{a_0, a_1\}$ given by the Fourier expansion coefficients of the transformation 3. Hence, even though our analytical model in principle applies to conductivity modulations derived from the conformal transformation, it accurately describes the simple sinusoidal modulations given in Eq. 2, provided that $\{a_0, a_1\}$ are chosen appropriately (see SM). Moreover, note that our analytical modelling applies to strong modulations of the order of the periodicity.

The optical response of the graphene metasurface in the subwavelength regime is derived by considering a plane wave normally incident on the modulated graphene, transforming it to the space where the graphene is homogeneously biased and imposing the boundary conditions for the EM fields, including the radiative reaction of the graphene conductivity grating (see Ref. 28 for details). This procedure yields the following complex transmission

and reflection coefficients at normal incidence,

$$r = \frac{\sqrt{\epsilon_1} - \sqrt{\epsilon_2} - \eta_0 \sigma_g(\omega) N_{\text{TO}}}{\sqrt{\epsilon_1} + \sqrt{\epsilon_2} + \eta_0 \sigma_g(\omega) N_{\text{TO}}}, \quad (4)$$

$$t = \frac{2\sqrt{\epsilon_1}}{\sqrt{\epsilon_2} + \sqrt{\epsilon_1} + \eta_0 \sigma_g(\omega) N_{\text{TO}}}. \quad (5)$$

where N_{TO} depends on frequency, geometrical parameters and dielectric environment, $N_{\text{TO}}(\omega, \gamma, w_0, b, \epsilon_1, \epsilon_2)$. In the SM we provide an analytical expression for N_{TO} in terms of the Fourier expansion coefficients of the conformal transformation and the electrostatic potential.

Figure 2 presents the optical response of the set of graphene metasurfaces with $\gamma = 400$ nm (period $1.2 \mu\text{m}$) under p-polarised normal incidence. The different modulation strengths considered in Fig. 1 are used here. Panel (a) plots transmittance and panel (b) absorption, as obtained from the analytical expressions for r and t , and with $T = \sqrt{\epsilon_1/\epsilon_2}|t|^2$, $R = |r|^2$ and $Q = 1 - R - T$. These analytical results are in excellent agreement with full wave simulations, as we discussed in Ref. 28. In all the spectra, the electric dipole mode [near field shown as an inset in panel (b)] features at a frequency slightly above 16 THz independently of the modulation strength. The reason for this can be traced back to the conformal transformation employed in designing the metasurface. All the metasurfaces belonging to the set characterised by a given γ (different w_0) relate to the same system through Eq. 3: a homogeneously biased graphene sheet. Since in the electrostatic limit the spectral properties of a plasmonic structure depend only on its geometry, all of them share the same plasmon resonance condition as a homogeneous graphene sheet of conductivity $\sigma_g(\omega)$,

$$\epsilon_1 + \epsilon_2 + \frac{4\pi\sigma_g(\omega)}{\omega}|k| = 0, \quad (6)$$

where k is the plasmon parallel momentum, *i.e.*, the wavevector component along x . On the other hand, the intensity and width of the peaks depends on the modulation strength. Transmittance at resonance decreases as w_0 increases, reaching suppressed transmission at $w_0 = 2.5$ for this set of parameters, while absorption reaches 0.5, the maximum possible

value for a symmetric system, for $w_0 = 1$ and then decreases. In addition, the transmission dips present a Fano shape that relates to the fact that these structures can also be mapped to a non-concentric annulus, a plasmonic structure that is well known for exhibiting a Fano response (see Ref. 40).

On the other hand, Eqs. 4 and 5 correspond to the reflection and transmission coefficients of a thin conducting sheet with effective electric conductivity given by

$$\sigma_{\text{eff}} = \sigma_g(\omega) N_{TO}(\omega, \gamma, w_0, b, y_0, \epsilon_1, \epsilon_2), \quad (7)$$

which fully justifies the interpretation of this system as a metasurface. The effective conductivity of the graphene metasurface, as obtained from the equation above, is shown in Fig. 2(c) (real part, blue solid line, and imaginary part, red dashed line) for a modulation strength that displays suppressed transmission, $w_0 = 2.5$. The effective conductivity presents a clear Lorentz resonant response, in agreement with the excitation of the plasmon dipole mode. Interestingly, a periodic modulation of the bias drastically modifies the response of a graphene monolayer, as can be seen by comparing the effective conductivity of the metasurface with the conductivity of a homogeneously biased graphene at the same chemical potential (real and imaginary parts plotted as solid and dashed thin lines, respectively).

While at normal incidence the set of metasurfaces defined by the periodicity $2\pi\gamma$ feature a dipolar plasmon resonance at the same frequency independently of the modulation strength, the response at angles of incidence $\theta \neq 0$ depends on w_0 . Figure 3(a) presents the optical response of the graphene metasurface considered in Fig. 2(c), under different angles of incidence. These spectra, calculated using full wave simulations, show that as the angle of incidence increases, the dipole peak in the spectrum develops a splitting. The reason for this is that the equivalence between the graphene with periodically modulated conductivity and the homogeneously doped graphene with plasmon dispersion given by Eq. 6 strictly holds only at $k = 0$, while at finite wave vectors the band structure of the graphene grating

displays a band gap – see Refs. 40 and 28. In addition, this band gap is larger for strongest modulations, implying that the distance between the two peaks in the spectrum depends on w_0 , in contrast with the peak position at normal incidence.

The effective conductivity of the sheet under non-normal incidence can be derived using a sheet retrieval method.⁴¹ In terms of the complex reflection and transmission coefficients, it reads as,

$$\sigma_{\text{eff}}^p = \frac{2}{\eta_0} \frac{\sqrt{\epsilon_2} \cos \theta_1 (1 - r) - \sqrt{\epsilon_1} \cos \theta_2 t}{\cos \theta_1 \cos \theta_2 (1 + r + t)}, \quad (8)$$

where $\theta_{2,1}$ are the angles of incidence and refraction [see sketch in Fig. 1(a)]. Figure 3(b) shows the real and imaginary parts of σ_{eff}^p (upper and lower panels, respectively) for the same metasurface as in Fig. 3(a). The retrieved effective conductivity clearly reflects the splitting in the optical spectrum by showing two distinct Lorentz resonance peaks. This result implies that the response of the graphene metasurface under study is sensitive to the angle of incidence of radiation, that is, it does not feature an isotropic response. Moreover, the response to incidence with s-polarisation is remarkably different to the p-polarisation one, as shown in Fig. 3(c), and which allows to switch between almost zero and almost perfect transmission by a simple change of polarization. The effective conductivity for s-polarisation, which can be retrieved using

$$\sigma_{\text{eff}}^s = \frac{2}{\eta_0} \frac{\sqrt{\epsilon_2} \cos \theta_2 (1 - r) - \sqrt{\epsilon_1} \cos \theta_1 t}{1 + r + t}, \quad (9)$$

does not present any resonant feature as s-polarised waves do not couple to surface plasmons. In this case, the effective conductivity of the modulated sheet is independent of the angle of incidence (see lower panel), as the incident radiation sees the modulated graphene as a sheet with averaged conductivity. The value of the effective conductivity can be obtained by averaging Eq. 2 over the unit cell, such that $\sigma_{\text{eff}}^s = \langle \sigma(x) \rangle = a_0 \sigma_g$, which is in perfect agreement with the conductivity retrieved from simulation results, at all angles of incidence.

Graphene with 2D conductivity modulation

In this Section we propose a graphene metasurface that presents an isotropic response to incident EM radiation. It is based on a graphene monolayer with a conductivity that is periodically modulated in a 2D arrangement, following

$$\sigma(x, y) = \sigma_g \left(a_0 + a_1 \sin \frac{x}{2\pi\gamma} \sin \frac{y}{2\pi\gamma} \right). \quad (10)$$

By modulating the conductivity in 2D, we aim at producing an isotropic optical response for arbitrarily polarised incident EM waves by providing plasmon coupling for both polarizations. Figure 4(a) shows the conductivity profile in a unit cell for a modulation strength of $w_0 = 2.5$, with $\{a_0, a_1\}$ in Eq. 10 chosen the same way as in 1D, for consistency. In order to deal with an arbitrary EM wave, we consider p and s-polarised waves, incident at an angle θ , and at a plane of incidence given by an azimuthal angle ϕ , see sketch in fig. 4(a). For p polarization, the incident field reads as

$$\mathbf{H}_{\parallel} = H_0(\sin \phi, \cos \phi) \exp [i(\mathbf{k}_{\parallel} \cdot \mathbf{r} + \mathbf{k}_{\perp} \cdot \mathbf{r})], \quad (11)$$

while for s-polarization we have

$$\mathbf{E}_{\parallel} = E_0(\sin \phi, \cos \phi) \exp [i(\mathbf{k}_{\parallel} \cdot \mathbf{r} + \mathbf{k}_{\perp} \cdot \mathbf{r})], \quad (12)$$

with $\mathbf{k}_{\parallel} = k_0\sqrt{\epsilon} \sin \theta (\cos \phi \mathbf{u}_x, \sin \phi \mathbf{u}_y)$ and $\mathbf{k}_{\perp} = k_0\sqrt{\epsilon} \cos \theta \mathbf{u}_z$.

In order to investigate the EM response of this metasurface, we first consider the case of normal incidence, $\theta = 0$, and with $\phi = 0$. We take the unit cell size as $1.25 \mu\text{m}$ and a modulation strength of $w_0 = 2.5$. The choice of the latter parameter is justified as it minimises on-resonance transmittance (see Fig. S3 in SM). It is worth noting here that, different to the graphene with 1D periodic conductivity modulation, in this case there is no conformal transformation that relates the set of metasurfaces with different w_0 to a simpler

system, and, for this reason, the position of the electrical dipole resonance redshifts with increasing w_0 . Fig. 4(b) shows the spectrum for a metasurface with the already mentioned parameters. Remarkably, for most part of the spectrum, the lines corresponding to p (solid) and s-polarized waves (dashed) lie on top of each other. Both polarisations display the same response to EM radiation, this is, they feature the same two absorption peaks (or transmittance dips). In addition, the agreement in frequency and line width of the low energy peak for both polarisations is remarkable. On the other hand, there is a slight shift in the second resonance peak for the different polarisations. The reason for this difference relates to the fact that, while the resonance frequency of the lower energy mode corresponds to a wavelength of $\lambda_0 \sim 8 \times 2\pi\gamma$, the higher energy mode has $\lambda_0 \sim 6 \times 2\pi\gamma$, meaning that the subwavelength unit cell requirement is best satisfied for the first peak.

From the field patterns shown in Fig. 4(b), it is clear that the two peaks in the spectrum correspond to a splitting of the electrical dipole mode: while the low energy peak corresponds to two dipoles oscillating in phase with the incident field, the high energy one corresponds to out-of-phase oscillation with it. Such a splitting emerges due to the fact that the metasurface is formed by a continuous graphene sheet with a modulated conductivity that ranges between a maximum value and a non-zero minimum. This situation is rather different to metasurfaces based on patterning graphene structures that also feature a dipolar response, such as nano islands²⁵ or cut-wires.¹⁶ To reinforce this interpretation we present the full spectrum which shows how the higher order modes also appear in pairs [see SM Fig. S4]. Furthermore, in Fig. S4(b) we include the reflectance spectrum, which presents the Fano shape, characteristic of the coupling between a highly localized mode (the dipolar resonances in the sub-wavelength high-conductivity region) and a continuous one (a surface plasmon polariton that propagates along the graphene sheet).

Let us now focus on the lower energy peak ($f \sim 30$ THz), which at normal incidence features the same response for both polarisations. Figure 5 presents the optical response and effective conductivity of the metasurface with the selected parameters from Fig. 4

under non-normal incidence (with $\phi = 0$) and for p and s polarisations [panels (a,b,c) and (d,e,f), respectively]. In contrast to the metasurface based on graphene with 1D conductivity modulation, the transmittance and absorption spectra do not develop a splitting, only a slight frequency shift. The reason for this can be related to the fact that the band corresponding to this mode is not very dispersive, as suggested by the large splitting between the two lower energy modes observed in Fig. S4. By appropriately designing the unit cell of this metasurface, we have removed the dependence of the spectrum on the angle of incidence. This is reflected in the effective conductivity retrieved from Eq. 8, which, for different θ , only differs by a slight frequency shift. In addition, the effective conductivity retrieved for s-polarised waves (using Eq. 9) shows a remarkable agreement with the one for p-polarisation, implying that this graphene metasurface behaves isotropically with respect to the incident angle for both polarisations. Regarding the dependence on the azimuthal angle, the effect of varying ϕ is only a slight frequency shift, see inset in panel (c).

Finally, it is worth noting that virtually perfect omnidirectionality can be achieved by considering deeply subwavelength unit cells. In the SM material we include the spectrum for a metasurface with the resonance peak at a wavelength of $\lambda_0 \approx 20 \times 2\pi\gamma$, much larger than the unit cell size. In this case, the retrieved effective conductivity for the low energy peak is virtually identical for all angles of incidence. While this feature is similar as the omnidirectional absorption found in graphene nano islands as those considered in Ref. 25, in this latter case there is only one dipolar peak in the spectrum even when a unit cell with a basis of two is considered. The reason for this is that the metasurface is formed by non-connected islands rather than a continuous graphene layer. This comparison adds to our interpretation of the peak splitting as aid by the plasmon propagating along the continuous graphene sheet. For more details on this comparison we refer the reader to the SM.

Conclusions

We have shown that a graphene sheet subject to a periodically modulated doping performs as a metasurface for incident radiation. We have first considered a 1D sinusoidal modulation of the sheet's conductivity, where analytical expressions for the optical spectrum at normal incidence are available from transformation optics. We have made use of such analytical formulae to optimise the performance of these graphene structures showing large transmission dips and absorption peaks, as well as to write an equation for the effective conductivity under p-polarised waves. On the other hand, s-polarised waves do not present a resonant response, which is in agreement with our interpretation of the resonances resulting from coupling of radiation to graphene plasmons.

In the second part of this work, we have proposed a metasurface that responds isotropically to radiation. By modulating the doping along two directions we have removed the dependence on the polarization, in both cases there is a grating in the direction of the electric field vector. We have shown that in this case the electric dipole mode is split in two resonances due to the interaction between the confined dipolar resonance and the surface plasmon propagating along the graphene sheet. We have shown that the lower energy mode of this splitting shows a remarkable agreement for both polarisations, while the higher energy one is more sensitive to the incident polarization. In addition, changing the angle of incidence results in effective conductivities that differ only by a slight frequency shift that can even be removed by going to metasurfaces with deep subwavelength unit cells (for instance ~ 300 nm for $\mu = 0.4$). Thus, the modulated graphene can be used for fast switching and tuning of THz radiation of arbitrary polarisation and orientation.

Acknowledgement

This work was supported by the Leverhulme Trust, the EPSRC (grant number EP/L024926/1) and the Gordon and Betty Moore Foundation. S.A. Maier additionally acknowledges the

Methods

Transformation optics

The analytical reflection and transmission coefficients of a graphene sheet with conductivity modulation in 1D are calculated with transformation optics. The procedure consists of mapping a space where a plane wave impinges normally on periodically doped graphene to a space where the graphene is homogeneously biased and a more complex wave is incident on it. This is achieved by means of the transformation given in Eq. (3). The optical response of the sheet is obtained by imposing the appropriate boundary conditions and including the radiative reaction of the graphene conductivity grating. This yields Eqs. (4) and (5) in the text, where the quantity N_{TO} reads

$$\begin{aligned}
 N_{\text{TO}} = 1 + \sum_{\substack{g=-\infty \\ g \neq 0}}^{\infty} |g|^2 & \left[i \text{sign}(g) (h_g^+ d_{2,-g}^+ e^{2|g|b} \right. \\
 & - h_g^- d_{2,-g} - e^{-2|g|b} - h_g^+ d_{2,-g}^- + h_g^- d_{2,-g}^+) \\
 & \left. - (h_g^+ + h_g^- e^{-2|g|b} e_{2,-g}^{\text{sca}}) \right] \quad (13)
 \end{aligned}$$

where d_g^\pm are the expansion coefficients of the conformal transformation, while the other coefficients correspond to the expansion of the electrostatic potential in the different regions of space. Full details on the derivation of this result can be found in Ref. 28.

Numerical simulations

Numerical simulations are carried out with a commercial finite element method solver (Comsol Multiphysics). In our calculations, graphene is introduced as a surface current, $\mathbf{J} = \sigma \mathbf{E}_{\parallel r}$, with σ given by Eqs. (2) or (10). Transmittance and reflectance through the structure are

measured in simulations of a single unit cell with periodic boundary conditions.

Supporting Information Available

Results for graphene metasurface with graphene parameters taken from experimental data, details on the conductivity modulation in 1D and transformation optics, and comparison to graphene nanoislands.

This material is available free of charge via the Internet at <http://pubs.acs.org/>.

References

1. Castro Neto, A. H.; Peres, N. M. R.; Novoselov, K. S.; Geim, A. K. The Electronic Properties of Graphene. *Reviews of Modern Physics* **2009**, *81*, 109–162.
2. Bonaccorso, F.; Sun, Z.; Hasan, T.; Ferrari, A. C. Graphene Photonics and Optoelectronics. *Nature Photonics* **2010**, *4*, 611–622.
3. Vafek, O. Thermoplasma Polariton within Scaling Theory of Single-Layer Graphene. *Physical Review Letters* **2006**, *97*, 266406.
4. Hanson, G. W. Dyadic Greens Functions and Guided Surface Waves for a Surface Conductivity Model of Graphene. *Journal of Applied Physics* **2008**, *103*, 064302.
5. Jablan, M.; Buljan, H.; Soljačić, M. Plasmonics in Graphene at Infrared Frequencies. *Physical Review B* **2009**, *80*, 245435.
6. Dubinov, A. A.; Aleshkin, V. Y.; Mitin, V.; Otsuji, T.; Ryzhii, V. Terahertz Surface Plasmons in Optically Pumped Graphene Structures. *Journal of Phys.: Condensed Matter* **2011**, *23*, 145302.
7. Koppens, F. H. L.; Chang, D. E.; García de Abajo, F. J. Graphene Plasmonics : A Platform for Strong Light-Matter Interaction. *Nano letters* **2011**, *11*, 3370–3377.

8. Nikitin, A. Y.; Guinea, F.; García-Vidal, F. J.; Martín-Moreno, L. Fields Radiated by a Nanoemitter in a Graphene Sheet. *Physical Review B* **2011**, *84*, 195446.
9. Fei, Z.; Andreev, G. O.; Bao, W.; Zhang, L. M.; S McLeod, A.; Wang, C.; Stewart, M. K.; Zhao, Z.; Dominguez, G.; Thiemens, M. *et al.* Infrared Nanoscopy of Dirac Plasmons at the Graphene-SiO₂ Interface. *Nano letters* **2011**, *11*, 4701–5.
10. Fei, Z.; Rodin, A. S.; Andreev, G. O.; Bao, W.; McLeod, A. S.; Wagner, M.; Zhang, L. M.; Zhao, Z.; Thiemens, M.; Dominguez, G. *et al.* Gate-Tuning of Graphene Plasmons Revealed by Infrared Nano-Imaging. *Nature* **2012**, *487*, 82–5.
11. Chen, J.; Badioli, M.; Alonso-González, P.; Thongrattanasiri, S.; Huth, F.; Osmond, J.; Spasenović, M.; Centeno, A.; Pesquera, A.; Godignon, P. *et al.* Optical Nano-Imaging of Gate-Tunable Graphene Plasmons. *Nature* **2012**, *487*, 77–81.
12. Maier, S. A. *Plasmonics: Fundamentals and Applications*; Springer: Boston, MA, 2007.
13. Ju, L.; Geng, B.; Horng, J.; Girit, C.; Martin, M.; Hao, Z.; Bechtel, H. A.; Liang, X.; Zettl, A.; Shen, Y. R. *et al.* Graphene Plasmonics for Tunable Terahertz Metamaterials. *Nature nanotechnology* **2011**, *6*, 630–634.
14. Tassin, P.; Koschny, T.; Soukoulis, C. M. Graphene for Terahertz Applications. *Science* **2013**, *341*, 620–621.
15. Low, T.; Avouris, P. Graphene Plasmonics for Terahertz to Mid-Infrared Applications. *ACS Nano* **2014**, *8*, 1086–1101.
16. Fan, Y.; Shen, N.-H.; Koschny, T.; Soukoulis, C. M. Tunable Terahertz Meta-Surface with Graphene Cut-Wires. *ACS Photonics* **2015**, *2*, 151–156.
17. Li, Z.; Yao, K.; Xia, F.; Shen, S.; Tian, J.; Liu, Y. Graphene Plasmonic Metasurfaces to Steer Infrared Light. *Scientific Reports* **2015**, *5*, 12423.

18. Smith, D. R.; Pendry, J. B.; Wiltshire, M. C. K. Metamaterials and Negative Refractive Index. *Science (New York, N.Y.)* **2004**, *305*, 788–92.
19. Soukoulis, C. M.; Wegener, M. Past Achievements and Future Challenges in the Development of Three-Dimensional Photonic Metamaterials. *Nature Photonics* **2011**, *5*, 523.
20. Kildishev, A. V.; Boltasseva, A.; Shalaev, V. M. Planar Photonics with Metasurfaces. *Science* **2013**, *339*, 1232009.
21. Ni, X.; Emani, N. K.; Kildishev, A. V.; Boltasseva, A.; Shalaev, V. M. Broadband Light Bending with Plasmonic Nanoantennas. *Science (New York, N.Y.)* **2011**, 50.
22. Yu, N.; Genevet, P.; Kats, M. A.; Aieta, F.; Tetienne, J.-P.; Capasso, F.; Gaburro, Z. Light Propagation with Phase Discontinuities: Generalized Laws of Reflection and Refraction. *Science (New York)* **2011**, *334*, 333–7.
23. Ding, F.; Wang, Z.; He, S.; Shalaev, V.; Kildishev, A. Broadband High-Efficiency Half-Wave Plate: A Super-Cell Based Plasmonic Metasurface Approach. *ACS nano* **2015**, 4111–4119.
24. Yin, X.; Ye, Z.; Rho, J.; Wang, Y.; Zhang, X. Photonic Spin Hall Effect at Metasurfaces. *Science* **2013**, *339*, 1405–1407.
25. Thongrattanasiri, S.; Koppens, F. H. L.; García De Abajo, F. J. Complete Optical Absorption in Periodically Patterned Graphene. *Physical Review Letters* **2012**, *108*, 047401.
26. Yan, H.; Li, X.; Chandra, B.; Tulevski, G.; Wu, Y.; Freitag, M.; Zhu, W.; Avouris, P.; Xia, F. Tunable Infrared Plasmonic Devices Using Graphene/Insulator Stacks. *Nature Nanotechnology* **2012**, *7*, 330–334.

27. Bludov, Y. V.; Peres, N. M. R.; Vasilevskiy, M. I. Graphene-Based Polaritonic Crystal. *Physical Review B* **2012**, *85*, 245409.
28. Huidobro, P. A.; Kraft, M.; Kun, R.; Maier, S. A.; Pendry, J. B. Graphene, Plasmons and Transformation Optics. *Journal of Optics* **2016**, *18*, 44024.
29. Alonso-González, P.; Nikitin, A. Y.; Golmar, F.; Centeno, A.; Pesquera, A.; Vélez, S.; Chen, J.; Navickaite, G.; Koppens, F.; Zurutuza, A. *et al.* Controlling Graphene Plasmons with Resonant Metal Antennas and Spatial Conductivity Patterns. *Science (New York, N.Y.)* **2014**, *344*, 1369–73.
30. Zhan, T. R.; Zhao, F. Y.; Hu, X. H.; Liu, X. H.; Zi, J. Band Structure of Plasmons and Optical Absorption Enhancement in Graphene on Subwavelength Dielectric Gratings at Infrared Frequencies. *Physical Review B* **2012**, *86*, 165416 (2012).
31. Slipchenko, T. M.; Nesterov, M. L.; Martin-Moreno, L.; Nikitin, A. Y. Analytical Solution for the Diffraction of an Electromagnetic Wave by a Graphene Grating. *Journal of Optics* **2013**, *15*, 114008.
32. Stauber, T.; Gómez-Santos, G.; De Abajo, F. J. Extraordinary Absorption of Decorated Undoped Graphene. *Physical Review Letters* **2014**, *112*, 077401.
33. Miao, Z.; Wu, Q.; Li, X.; He, Q.; Ding, K.; An, Z.; Zhang, Y.; Zhou, L. Widely Tunable Terahertz Phase Modulation with Gate-Controlled Graphene Metasurfaces. *Physical Review X* **2015**, *5*, 041027.
34. Zhao, B.; Zhang, Z. M. Strong Plasmonic Coupling between Graphene Ribbon Array and Metal Gratings. *ACS Photonics* **2015**, *2*, 1611–1618.
35. Nikitin, A. Y.; Guinea, F.; Garcia-Vidal, F. J.; Martin-Moreno, L. Surface Plasmon Enhanced Absorption and Suppressed Transmission in Periodic Arrays of Graphene Ribbons. *Physical Review B* **2012**, *85*, 081405(R).

36. Nikitin, A. Y.; Guinea, F.; Martin-Moreno, L. Resonant Plasmonic Effects in Periodic Graphene Antidot Arrays. *Applied Physics Letters* **2012**, *101*, 151119.
37. Fang, Z.; Thongrattanasiri, S.; Schlather, A.; Liu, Z.; Ma, L.; Wang, Y.; Ajayan, P. M.; Nordlander, P.; Halas, N. J.; García De Abajo, F. J. Gated Tunability and Hybridization of Localized Plasmons in Nanostructured Graphene. *ACS Nano* **2013**, *7*, 2388–2395.
38. Fang, Z.; Wang, Y.; Schlather, A. E.; Liu, Z.; Ajayan, P. M.; García De Abajo, F. J.; Nordlander, P.; Zhu, X.; Halas, N. J. Active Tunable Absorption Enhancement with Graphene Nanodisk Arrays. *Nano Letters* **2014**, *14*, 299–304.
39. Forati, E.; Hanson, G. W.; Yakovlev, A. B.; Alù, A. Planar Hyperlens Based on a Modulated Graphene Monolayer. *Physical Review B - Condensed Matter and Materials Physics* **2014**, *89*, 1–5.
40. Kraft, M.; Luo, Y.; Maier, S. A.; Pendry, J. B. Designing Plasmonic Gratings with Transformation Optics. *Physical Review X* **2015**, *5*, 031029.
41. Tassin, P.; Koschnya, T.; Soukoulis, C. M. Effective Material Parameter Retrieval for Thin Sheets: Theory and Application to Graphene, Thin Silver Films, and Single-Layer Metamaterials. *Physica B* **2012**, *407*, 4062–4065.

Graphical TOC Entry

Graphene has received a lot of interest in recent years as an alternative plasmonic platform. Its unique optical properties result in electrically tunable plasmons that allow for extreme confinement of electromagnetic energy in the technologically significant regime of THz frequencies. Here we add an extra degree of freedom by using graphene as a metasurface, proposing to dope it with an electrical gate patterned in the micron or sub-micron scale. First, we show a metasurface with unusual properties such as Dirac points, that we study analytically. Then, we design a versatile metasurface with a tunable isotropic response.

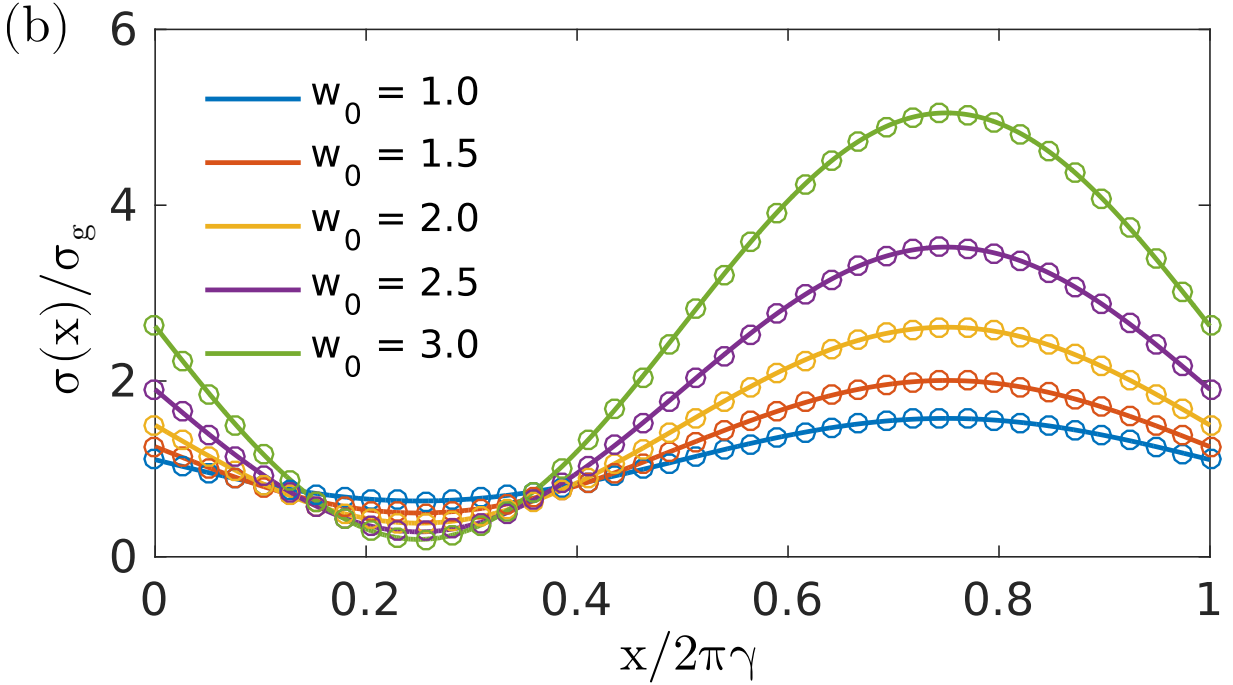
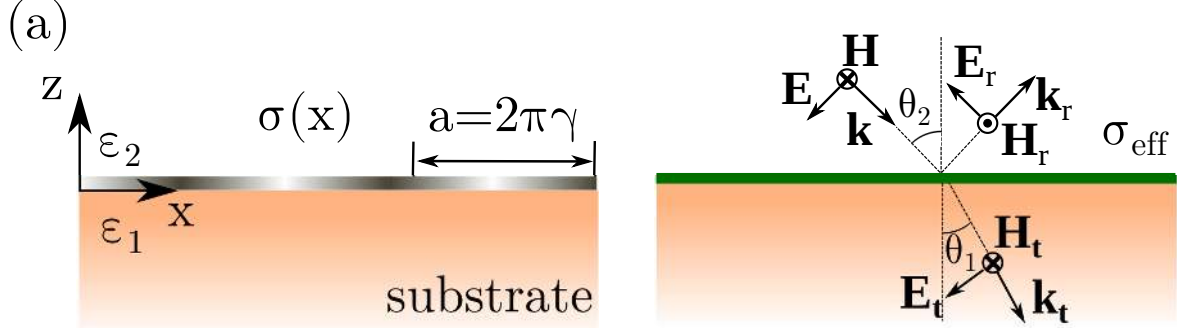


Figure 1: Metasurface with periodically modulated graphene. (a) Sketch of the monolayer graphene structure. The conductivity of the graphene sheet is periodically modulated along one direction, $\sigma(x)$, with period $2\pi\gamma$ (left panel). For radiation of relevant wavelengths, the graphene appears as a homogeneous sheet with effective conductivity σ_{eff} . (b) Conductivity modulation profile for several values of the modulation strength, w_0 .

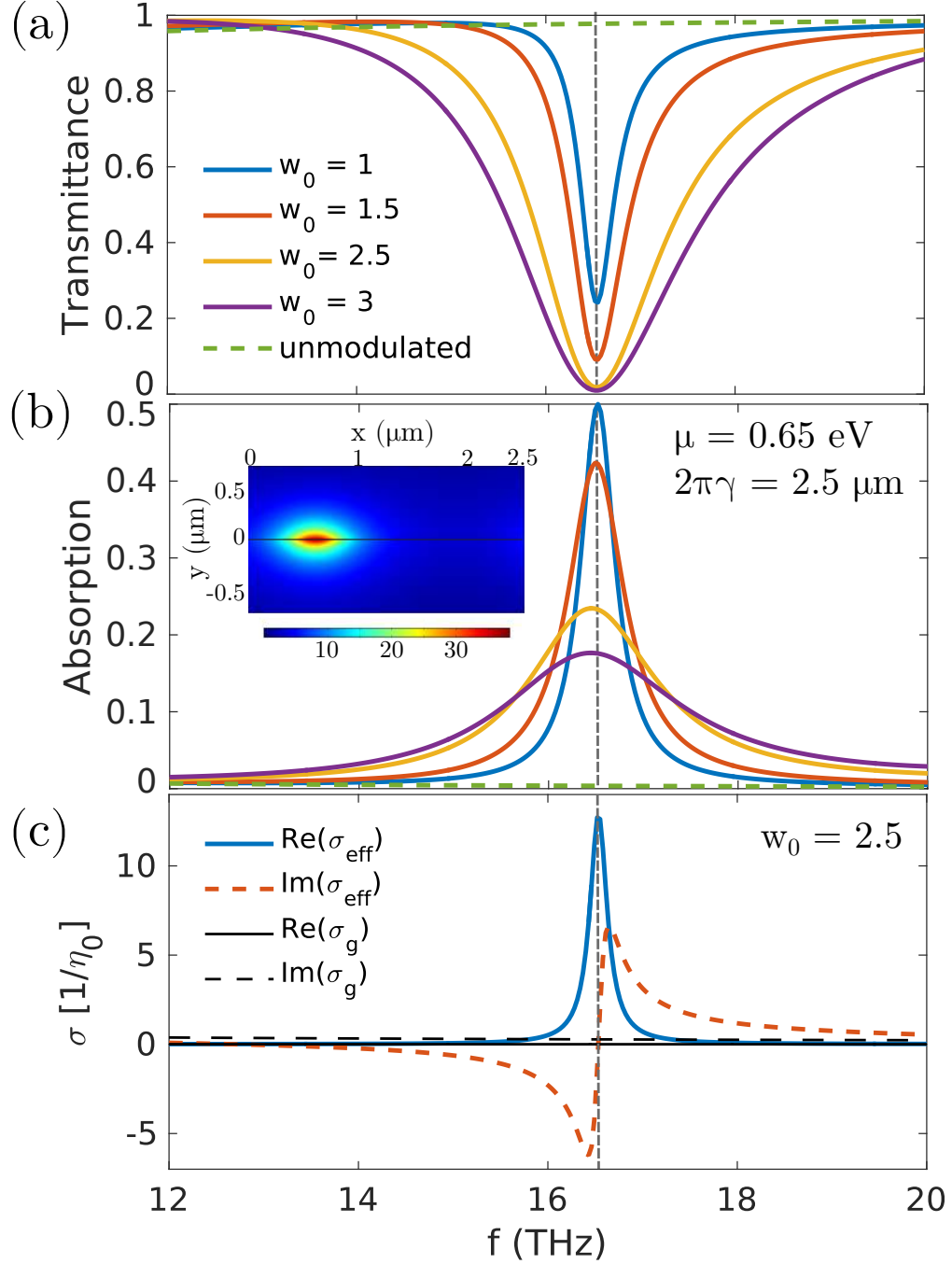


Figure 2: Tunable graphene metasurface for p-polarised waves. Analytical transmission (a) and absorption (b) spectra at normal incidence for metasurfaces of periodicity $2\pi\gamma$ with $\gamma = 400$ nm, and placed in a symmetric environment $\epsilon_1 = \epsilon_2 = 1$. Different modulation strengths are shown, as well as the spectrum of homogeneously biased graphene (dashed lines). Inset panel in (b): simulated field enhancement normalized to the norm of the incident electric field for $w_0 = 2.5$ and at the resonance frequency. (c) Effective surface conductivity for the case with $w_0 = 2.5$.

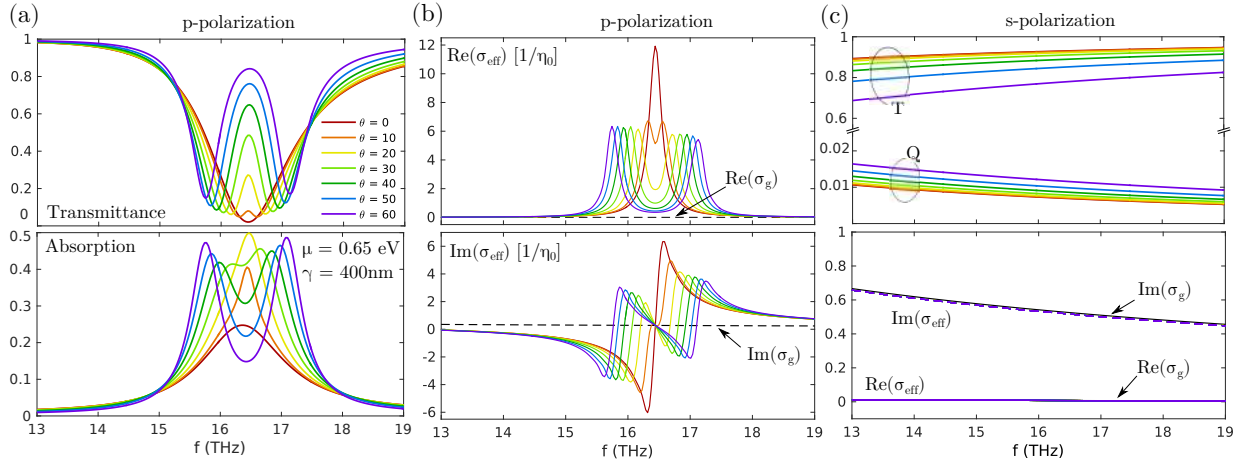


Figure 3: Graphene metasurface with $\gamma = 400$ nm and $w_0 = 2.5$ for p-polarised waves at non-normal incidence. (a) Optical spectrum, transmittance –upper panel– and absorption –lower panel– for different angles of incidence, θ . (b) Retrieved effective conductivity: real and imaginary parts are displayed in the upper and lower panel, respectively. (c) Optical response [transmittance (solid line) and absorption (dashed line)] and effective conductivity [real and imaginary parts (solid and dashed lines, respectively)] for s-polarised EM waves. Note that the lines corresponding to all incident angles lay on top of each other. The thin black lines correspond to $\langle \sigma(x) \rangle = a_0 \sigma_g$.

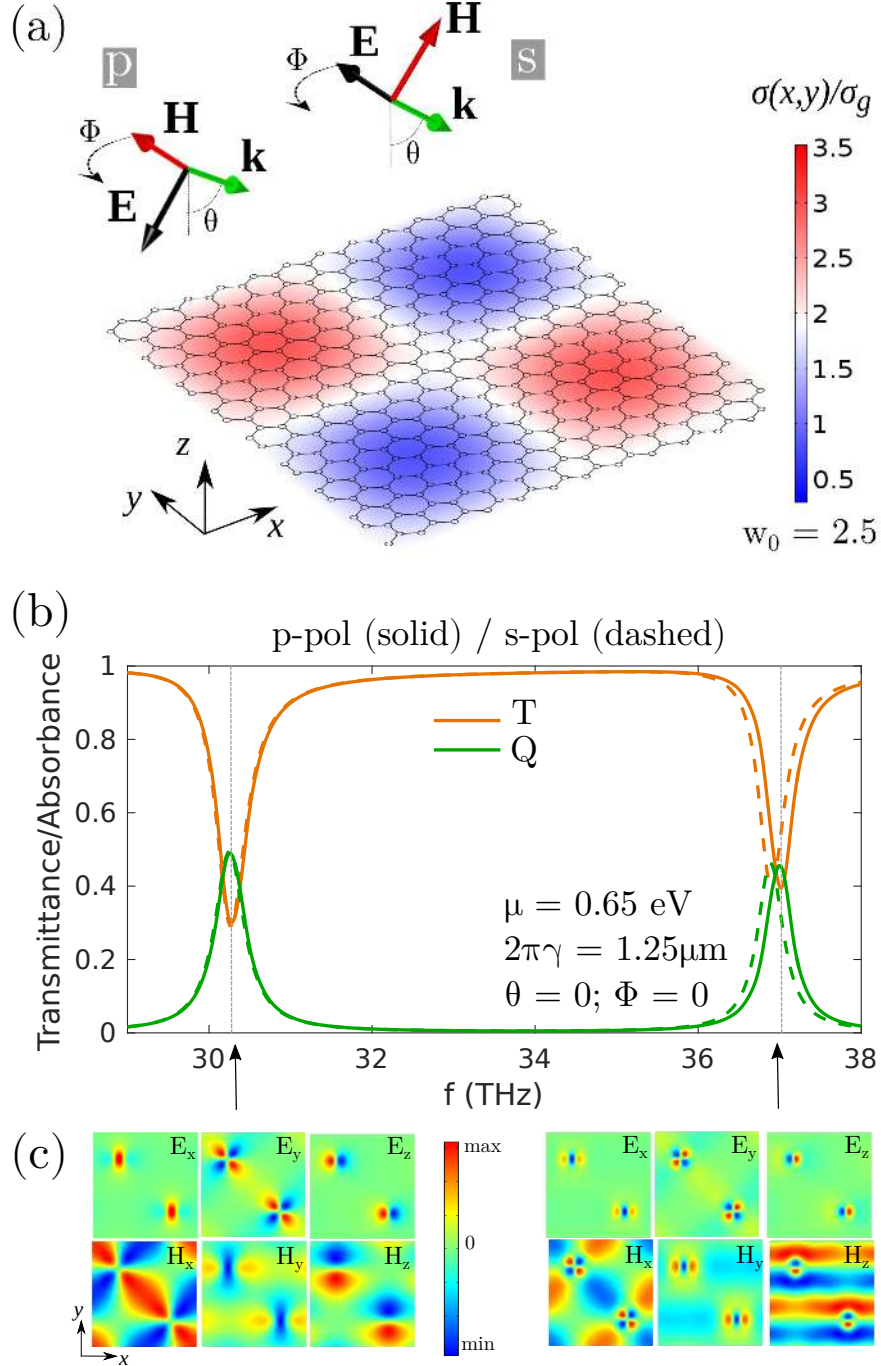


Figure 4: Graphene with 2D conductivity modulation. (a) Schematics of the unit cell and wave incidence for s and p polarisation. The conductivity profile $\sigma(x,y)$ is shown for the case $w_0 = 2.5$. (b) Simulated transmission and absorption spectra (upper and lower panels) for different values of the modulation strength. Normal incidence ($\theta = 0$), p-polarisation and $\phi = 0$ is considered. The periodicity of the structure is $2\pi\gamma$, with $\gamma = 200$ nm, and it is embedded in a symmetric environment $\epsilon_1 = \epsilon_2 = 1$. (c) Field plots in the unit cell at each resonance for p-polarization. Note that the color scale is different for each case, with E_x and E_z being the dominant electric field components, and H_x and H_z the magnetic field ones. Electric fields for s-polarization show the same patterns but exchanging E_x for E_y and with a 90° rotation.

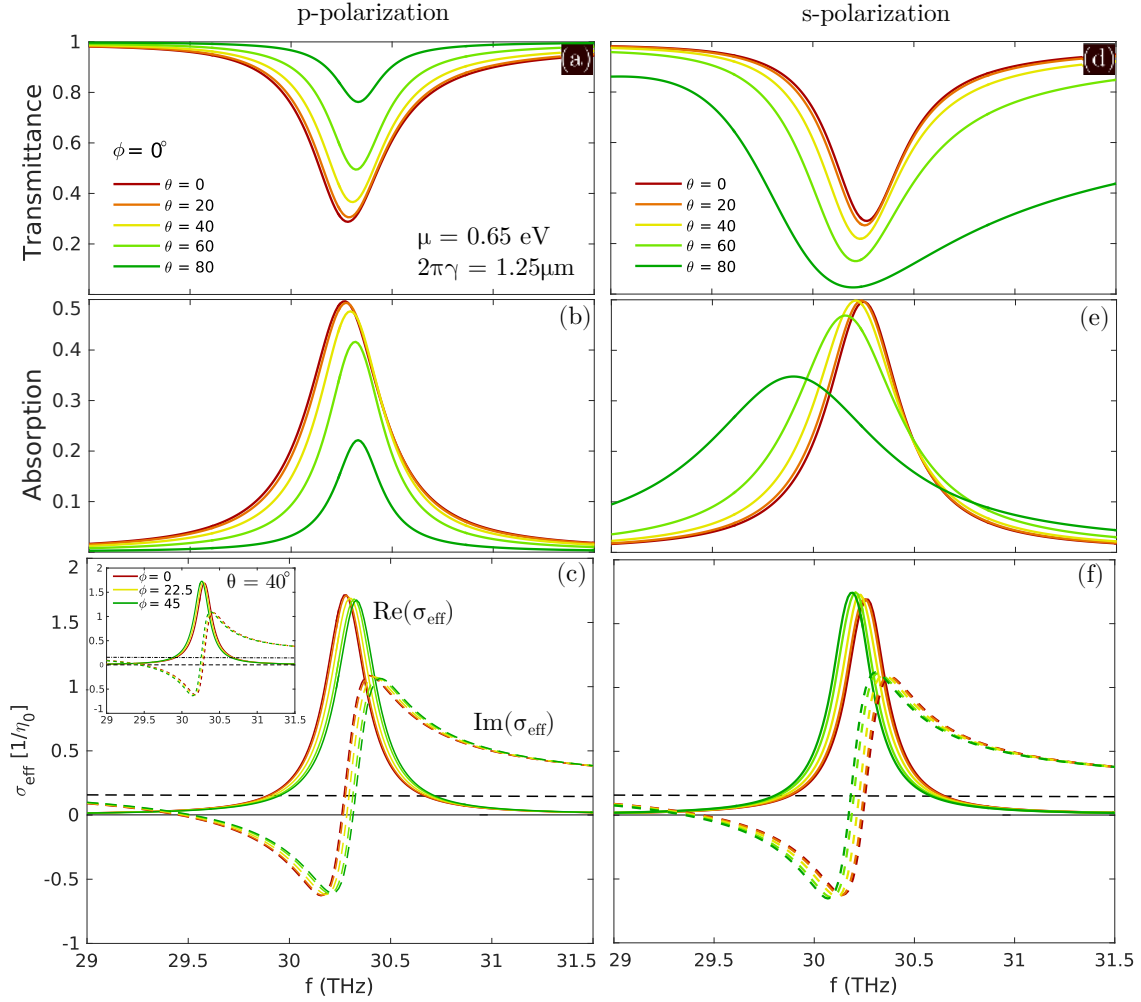


Figure 5: Isotropic graphene metasurface for both polarisations. The unit cell parameters are $2\pi\gamma = 200\text{ nm}$ and $w_0 = 2.5$, as in Fig. 3. Transmittance (a/d), absorption (b/e) and effective conductivity (c/f) for p/s-polarizations and for different angles of incidence θ . The azimuthal angle is fixed at $\phi = 0$. Variation with ϕ is shown as an inset panel (c).

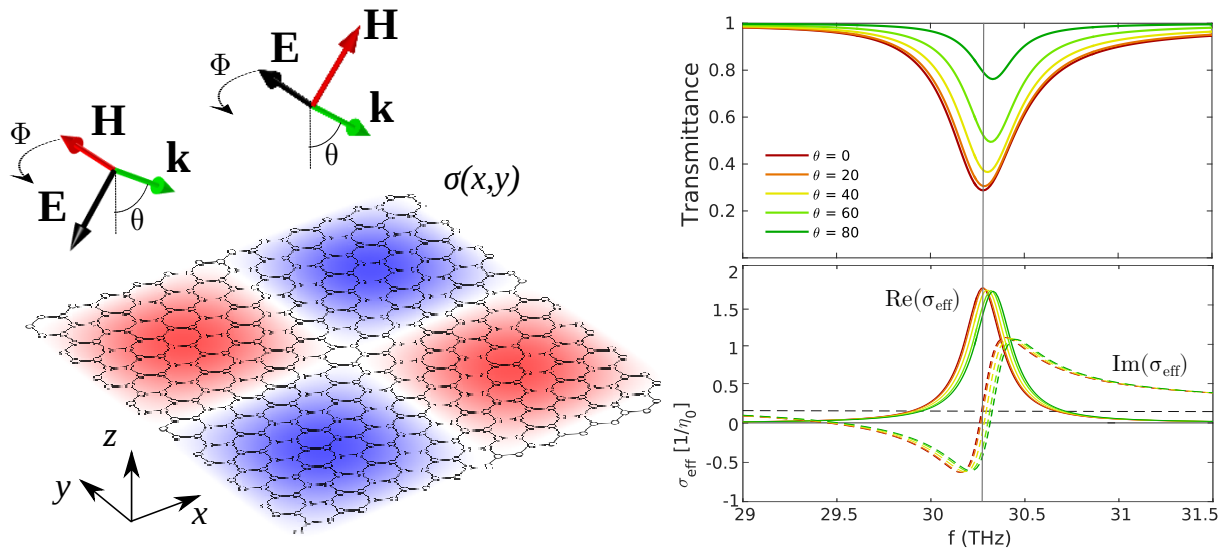


Figure 6: For table of contents only.